Machine Learning-Based Detection of Land Use and Land Cover Change in Phu Quoc Special Zone, An Giang Province, Vietnam, Using Google Earth Engine

Mai, L. C.
Faculty of Applied Biology, Tay Do University, 68 Tran Chien Street, Thanh My Area, Cai Rang Ward, Can Tho City, Vietnam, E-mail: mlcanh@tdu.edu.vn, ORCID ID: 0009-0000-1331-3397
DOI: https://doi.org/10.52939/ijg.v22i10.5241

Abstract
Phu Quoc Special Zone is one of the most developed island destinations in Vietnam. The island has undergone significant land use and land cover (LULC) changes due to urbanization, infrastructure development, and tourism. The objective of this study is to analyze LULC changes from 1995 to 2025 in Phu Quoc usiing Landsat satellite imagery and machine learning (ML) algorithms on the Google Earth Engine (GEE) platform. Four ML algorithms, namely Random Forest, Classification and Regression Tree, Gradient Tree Boosting, and Support Vector Machine, were employed to identify distinct LULC classes, including forest, agricultural land, built-up area, bare land and water body. The classification results yielded an overall accuracy ranging from 85.24 ± 2.81% to 94.41 ± 1.59% and Kappa coefficients ranging from 0.80 ± 0.03 to 0.93 ± 0.02 across the analyzed years, indicating that RF outperformed the other algorithms. Although forest remained the most dominant LULC class, its area decreased by 11.56% over the study period. Conversely, built-up area expanded rapidly by 627.72%, primarily through conversion from forest, agricultural land, and bare land, highlighting the profound impacts of urbanization, infrastructure development, and tourism on LULC changes. The findings demonstrate the effectiveness of integrating ML algorithms within the GEE platform for long-term LULC monitoring. The identified LULC changes provide valuable spatial information to support land-use planning, management, and sustainable land use.

Keywords: Google Earth Engine, Landsat, LULC, Machine Learning, Phu Quoc

1. Introduction

Land use and land cover (LULC) change is one of the primary drivers of global environmental change [1] and [2], while profoundly impacting environmental sustainability, socio-economic development, and spatial planning [3]. Over the past few decades, LULC changes have contributed to biodiversity loss, accelerated climate change, and the degradation of natural resources [4]. Furthermore, intensifying urbanization, infrastructure development, and tourism have significantly accelerated LULC changes, particularly in coastal islands and global tourist destinations [5] and [6]. These changes have led to the expansion of built-up area and the decline of natural forests, agricultural land, and ecosystems, thereby contributing to alterations in landscape structure and ecological functions [7]. For tourism islands characterized by limited land resources and vulnerable ecosystems, accurate monitoring and assessment of LULC changes serve as a crucial foundation for supporting resource management, environmental conservation, and sustainable development planning [8]. In Vietnam, Phu Quoc Special Zone (Phu Quoc) has emerged as one of the most attractive destinations for economic investment and tourism. With its strategically important location and rich natural resources, Phu Quoc aims to become a major marine economic center, with a particular focus on the service economy [9]. Over the past three decades, Phu Quoc has experienced rapid socio-economic growth, characterized by intensive infrastructure development, urban expansion, the construction of tourism-related facilities, and population growth. Large-scale investments in transportation networks, residential areas, resorts, and commercial centers have significantly transformed the island's landscape [10]. These activities have driven LULC transitions and significantly altered the natural landscape. Increasingly, forest areas and agricultural land are being converted into built-up area, residential zones, infrastructure, and tourism service facilities [11]. To effectively manage and minimize the negative

impacts of land use, the Government has implemented land-use planning on a 10-year cycle, while simultaneously establishing long-term strategic orientations covering up to 30 years [12]. The development and adjustment of land-use planning require information on past land-use changes. Therefore, historical LULC maps are essential for quantifying the extent and identifying trends in land use change. They also help determine future land-use patterns and their spatial dynamics [13].

A major challenge in LULC changes analysis is the lack or limited availability of GIS data, particularly for historical periods several decades ago, as in the case of Phu Quoc [14]. Therefore, remote sensing has become an effective tool for monitoring LULC changes due to its cost-effectiveness, wide-area coverage, and availability of various spatial, temporal, and spectral resolutions [15] and [16]. However, accurately identifying LULC from remote sensing imagery remains a challenge due to the complexity of spectral characteristics and the heterogeneity of the land surface [17]. Accordingly, machine learning (ML) methods have been increasingly applied on the Google Earth Engine (GEE) platform for LULC classification, with results showing higher reliability than traditional classification methods. Algorithms such as Random Forest (RF), Classification and Regression Tree (CART), Gradient Tree Boosting (GTB), Support Vector Machine (SVM), and others are capable of processing complex and high-dimensional remote sensing imagery while improving the accuracy and stability of classification [18]. Although these ML algorithms have proven effective and are widely adopted for mapping LULC in many regions around the world [19], no study has evaluated and compared the performance of these ML algorithms to support the selection of an optimal algorithm in Phu Quoc.

The main objective of this study is to assess LULC changes in Phu Quoc from 1995 to 2025, using GEE and four ML algorithms (RF, CART, GTB, and SVM). The specific objectives focus on: (1) comparing the reliability of the four ML algorithms in LULC classification and (2) detecting LULC changes in Phu Quoc over three decades, providing a reliable database to support sustainable land-use planning and resource management.

2. Study Area

Phu Quoc is the largest island in Vietnam, situated off the country's southwestern coast in the Gulf of Thailand, the island extends between 10°01′N and 10°27′N latitude and between 103°51′E and 104°05′E longitude (Figure 1), covering a total area of approximately 566.84 km².

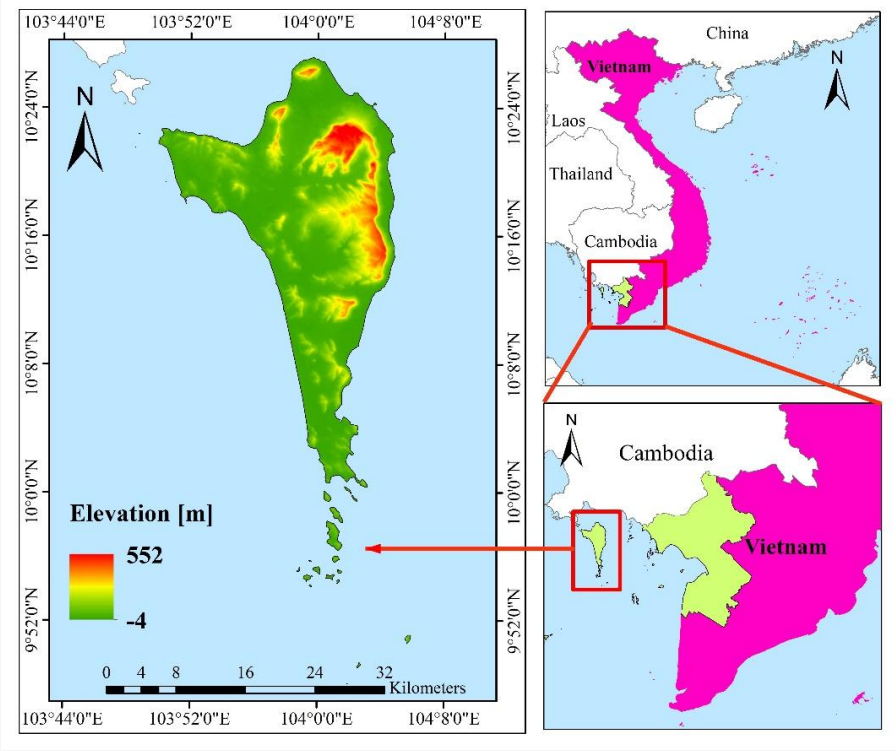


Figure 1: Phu Quoc special zone, Vietnam

Prior to the 2025 administrative reorganization, Phu Quoc was administratively part of Kien Giang Province. Following the reorganization, Phu Quoc is now administratively part of An Giang Province [20]. Phu Quoc features a diverse topography consisting of low mountain ranges interspersed with narrow coastal plains. The island is renowned for its rich biodiversity, abundant marine resources, and compelling natural landscapes, rendering it one of Vietnam's most vital ecological destinations. Its pristine beaches and thriving marine ecosystems are essential for both environmental conservation and economic development. Additionally, the tropical monsoon climate, characterized by relatively stable temperatures and ample sunshine year-round, fosters tourism and various outdoor economic activities [9]. Most of the island's area is covered by natural forest ecosystems, including Phu Quoc National Park, a protected area. Phu Quoc has experienced a marked increase in population in recent years, mainly due to the rapid growth of tourism. Parallel to this trend, accelerating urbanization and large-scale infrastructure development including resorts, transportation networks, and urban amenities have led to significant LULC changes. The most notable transitions involve the conversion of forest and agricultural land into built-up area [10]. Currently, Phu Quoc exhibits diverse LULC types, including forest, agricultural land, built-up area, bare land and water body. These alterations have not only reshaped the spatial structure of land use but have also impacted the island's natural resources and ecosystems. Given its high ecological, economic, and tourism value, Phu Quoc serves as an ideal case study for investigating LULC changes within the context of rapidly developing tropical coastal islands.

3. Methodology

This study evaluates the performance of different ML algorithms for analyzing LULC changes in Phu Quoc from 1995 to 2025. The overall methodological framework is illustrated in Figure 2.

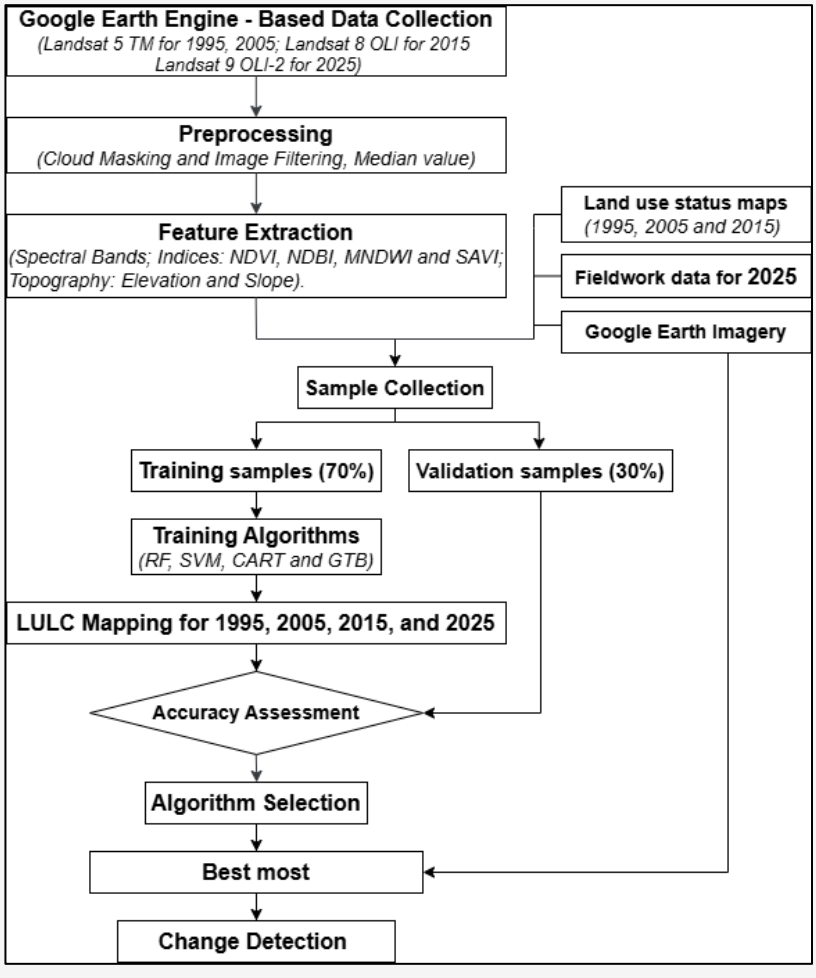


Figure 2: LULC change study workflow

Table 1: Characteristics of the Landsat Imagery used in this study

Parameter	Landsat 5-TM		Landsat 8-OLI	Landsat 9-OLI2
	1995	2005	2015	2025
Date of acquisition	08/01; 21/01; 09/02; 13/3;	03/01; 19/01; 08/02; 08/4;	15/01; 31/01; 16/02; 20/3; 05/4; 21/4	02/01; 18/01; 03/02; 27/02; 23/3; 08/4
Resolution (m)	30	30	30	30
Band	1, 2, 3, 4, 5, 7	1, 2, 3, 4, 5, 7	2, 3, 4, 5, 6, 7	2, 3, 4, 5, 6, 7
GEE Asset ID	LANDSAT/LT05/ C02/T1_L2	LANDSAT/LT05/ C02/T1_L2	LANDSAT/LC08/ C02/T1_L2	LANDSAT/LC09/ C02/T1_L2

3.1 Datasets Used

3.1.1 Image preprocessing

Landsat Imagery were freely available from the USGS [21] and accessed through the GEE platform to analyze LULC changes in 1995, 2005, 2015, and 2025. Due to Phu Quoc's tropical monsoon climate, satellite images frequently exhibit high cloud cover, particularly during the rainy season. Therefore, a stringent image selection protocol was implemented to ensure high-quality data; only images acquired during the dry season (from January to April of each respective year) were selected. Furthermore, scenes with cloud cover exceeding 30% were excluded to guarantee data quality and improve classification accuracy. A total of 20 Landsat scenes were collected throughout the study period (Table 1).

Surface Reflectance Conversion: To ensure consistency among the Landsat imagery, we first used the Landsat Collection 2 Level-2 Surface Reflectance products as the input data. The *DN* values of the surface reflectance bands were converted into surface reflectance values using Equation 1 [22].

$$SR = DN \times 0.0000275 - 0.2$$

Equation 1

Where *SR* is the surface reflectance value, and *DN* is the integer value stored in the Collection 2 Level-2 product. The corresponding spectral bands between Landsat 5-Thematic Mapper (TM), Landsat 8-Operational Land Imager (OLI) and Landsat 9-Operational Land Imager 2 (OLI2) were used to construct a unified set of variables consisting of Blue, Green, Red, NIR, SWIR-1, and SWIR-2. This approach helps maintain the consistency of the input variables in the multi-temporal LULC changes analysis.

Cloud and Cloud-Shadow Masking: All Landsat imagery were subjected to QA masking using the QA_PIXEL and QA_RADSAT bands from the Landsat Collection 2 Level-2 products. Pixels with clouds and cloud shadows in QA_PIXEL were removed. In addition, pixels saturated in the spectral bands were also removed using QA_RADSAT. This contributes to reducing the effects of clouds and cloud shadows, ensuring consistency among the study years in Phu Quoc.

Topographic Correction: Because Phu Quoc has mountainous terrain, particularly in the northeastern and eastern parts, topographic correction was applied using the C-correction method based on solar geometry parameters derived from the Landsat metadata and a 30-m digital elevation model (DEM) (Equation 2) [23].

$$\rho H = \rho T \left(\frac{\cos \theta_z + C}{IL + C} \right)$$

Equation 2

Where ρH is the surface reflectance value; ρT is the estimated reflectance of the sloped surface and is calculated as $\rho T = b + mIL$; θ_z is the solar zenith angle; IL is the illumination condition calculated from the solar zenith angle, solar azimuth angle, slope, and aspect; the C coefficient is specific to each spectral band: $C = b/m$; b and m are the intercept and slope, respectively, of the linear regression between illumination and reflectance for each spectral band.

Annual Median Composite: The selected Landsat imagery were preprocessed and subsequently composited using the pixel-based median composite method on the GEE platform to generate a single composite image for each study year. This method aims to contribute to reducing the effects of residual clouds, random noise, and differences among image scenes. The annual composite images were then used as input data for LULC classification in Phu Quoc.

Spectral Band Harmonization: To ensure spatial and temporal consistency between Landsat 5-TM, Landsat 8-OLI and Landsat 9-OLI2, the corresponding spectral bands were matched according to their spectral ranges and functions in the study. The image band values and spectral indices were applied to all study years, including Blue, Green, Red, NIR, SWIR-1, SWIR-2*, NDVI, MNDWI,*

NDBI, and *SAVI*. All Landsat datasets were processed following the same Surface Reflectance workflow, with cloud and cloud-shadow masking, topographic correction, and annual median compositing performed sequentially. Although differences exist in the values and processing algorithms between TM and OLI/OLI-2, the use of corresponding spectral bands helps minimize differences among sensors and ensures consistency when comparing LULC among years.

3.1.2 Auxiliary data

In addition to satellite imagery, several GIS datasets for the Phu Quoc area were collected to support the training/validation samples, LULC analysis, and interpretation. These datasets included administrative boundaries, road networks, rivers and streams, digital elevation data, Google Earth imagery, and land-use status maps provided by local authorities (Table 2). Due to the complex topography of Phu Quoc, two topographic variables, elevation and slope were also included as ancillary variables for LULC classification. These variables were derived from the ALOS Digital Elevation Model (DEM) with a spatial resolution of 30 m × 30 m, obtained from the Japan Aerospace Exploration Agency (Table 2). Previous research has indicated a close relationship between topographic factors and the spatial distribution of LULC types. [24].

3.1.3 Ground-truth data

Field surveys conducted in May and June 2025 provided ground-truth data collected using a Garmin GPSMAP 65S device. Based on the 30 × 30 m spatial resolution of the Landsat imagery, we planned the field survey routes by navigating the road network within the study area, as visualized in Google Earth. A total of 100 sampling sites were randomly selected to represent the LULC types in the study area (Figure 3(a)), while sample locations derived from the Landsat imagery (Figure 3(b)). Images of the LULC classes were captured during our field surveys (Figure 3(c)). Additionally, we conducted interviews with local authorities, farmers, forestry staff, and long-term residents, individuals with extensive knowledge of LULC changes in Phu Quoc, to identify temporally stable (invariant) locations that could support the selection of training/validation samples for the historical years (1995, 2005, and 2015). The field survey was conducted after the 2025 remote sensing imagery acquisition period. This time lag was considered unlikely to substantially affect the classification of relatively stable agricultural land in Phu Quoc, where the majority of cultivated areas consist of perennial crops, such as black pepper plant, *Rhodomyrtus tomentosa*, and fruit trees, which remain relatively stable over short periods. For bare land and other areas susceptible to land cover changes, we conducted additional verification using high-resolution imagery available on Google Earth and conducted interviews to verify the classification and minimize discrepancies arising from the time gap between image acquisition and field surveys.

3.2 LULC Classification

3.2.1 Training data and sample design

In this study, LULC classes were defined following the Vietnamese regulatory framework for establishing and updating current land-use status maps [25]. The study area was classified into five LULC classes: Forest, agricultural land, built-up area, bare land, and water body (Table 3 and Figure 3). Before using the reference maps, we performed geometric correction. The purpose was to ensure the best spatial alignment and accurate matching among the datasets: Landsat imagery, land-use status maps, and other spatial datasets were transformed into the WGS 84/UTM Zone 48N coordinate reference system using the nearest-neighbor resampling algorithm. The maps were geometrically corrected using 30 to 35 ground control points (GCPs), and geometric accuracy was assessed using the root mean square error (RMSE). An RMSE of less than 0.5 pixels was obtained, which was considered acceptable for the geometric correction process [26].

Table 2: Ancillary data used in this study

Data	Resolution	Date of acquisition	Source
Land-use status maps	1:25.000	2005 2015	An Giang Department of Agriculture and Environment
Google Earth Imagery	-	2015 2025	https://www.google.com/earth (Accessed on Nov. 20, 2025)
Ground-truth data	-	May - June 2025	Field survey (100 field observations)
ALOS DEM	30 × 30 m	1995-2025	https://www.eorc.jaxa.jp (Accessed on Nov. 20, 2025)
Road	-	2025	https://www.openstreetmap.org (Accessed on Nov. 20, 2025)
River and canal	-	2025	

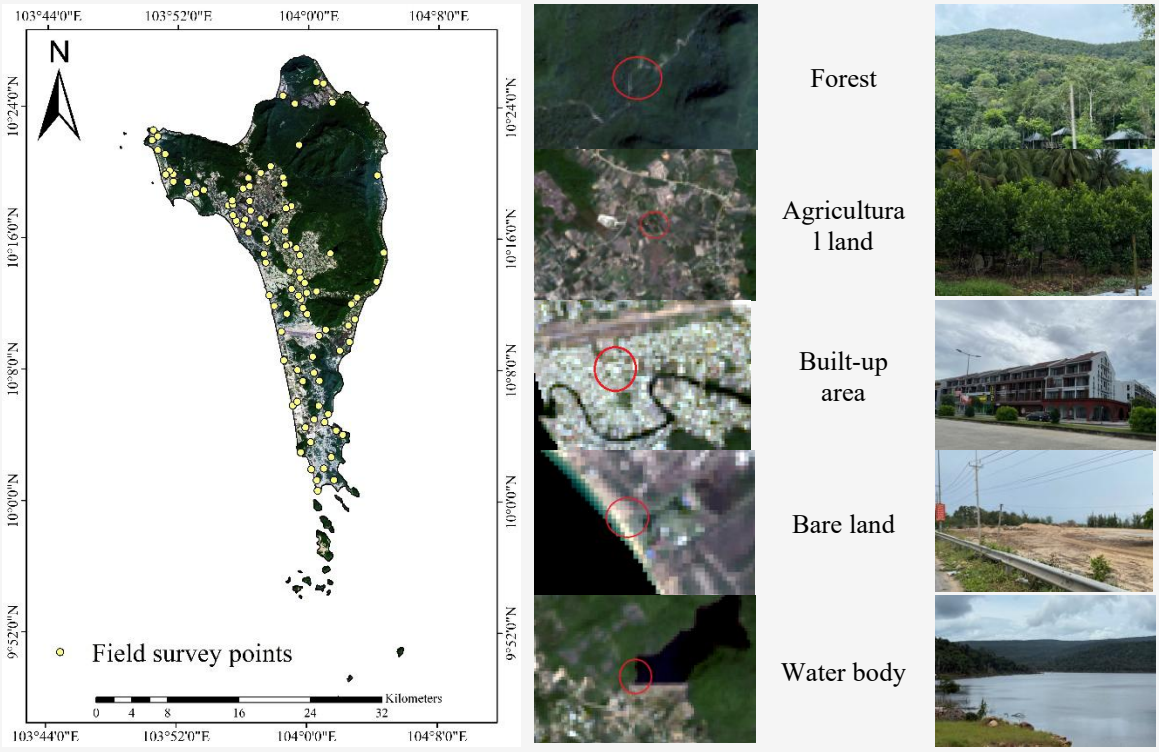


Figure 3: Field survey data:
(a) locations of field survey points, (b) Landsat imagery samples, and (c) field photographs of LULC classes

Table 3: LULC classification and descriptions for the study area

LULC	Description
Forest	Areas predominantly covered by trees forming closed canopies, including natural forests, plantations, and mixed forest land
Agricultural land	Areas covered with perennial and annual crops and irrigated areas
Built-up area	Urban areas, residential, commercial, roads, industrial and other man-made structures.
Bare land	Areas without vegetation cover, including exposed fallow land, beaches, and sandy areas
Water body	Rivers, canals, ponds, lakes, and shallow coastal waters within the study area

Supervised classification requires the preparation of training and validation datasets to ensure the reliability of the classification results. In this study, samples for 1995, 2005, 2015, and 2025 were selected using the 1:25,000 current land-use map, Google Earth imagery, DEM, road network, and river and canal data available for the study area. Samples were selected using the stratified random sampling method proposed by [27]. First, the Landsat imagery for 1995, 2005, 2015, and 2025 were overlaid with the aforementioned ancillary datasets in ArcGIS. Subsequently, temporally stable (invariant) areas representing the five LULC classes were identified. Polygons were then delineated around the centers of these areas to minimize edge effects. The selected LULC sample locations were subsequently cross-checked against the aforementioned ancillary datasets, as well as previously collected field data to verify their class labels. A total of 600 samples representing the five LULC classes were generated for 1995, 2005, and 2015. For 2025, a total of 500 samples were generated using the same map-based procedure, while 100 samples were collected during fieldwork. The training samples were allocated among the LULC classes according to their spatial distribution, area coverage, and spectral characteristics in each study year. Accordingly, the number of samples assigned to individual LULC classes varied to ensure adequate representation of their spatial and spectral variability, while the total number of samples was maintained at 600 for each year (Table 4).

Table 4: Annual sample points divided into training and validation datasets

Year	Training samples						Year	Validation samples					
	FR	AL	BA	BL	WB	Total		FR	AL	BA	BL	WB	Total
1995	175	105	35	63	42	420	**1995**	**75**	45	15	27	18	180
2005	175	105	49	49	42	420	**2005**	75	45	21	21	18	180
2015	154	105	70	49	42	420	**2015**	66	45	30	21	18	180
2025	154	105	70	49	42	420	**2025**	66	45	30	21	18	180

Note: FR (Forest), AL (Agricultural land) BA (Built-up area), BL (Bare land) and WB (Water body).

For each study year, 70% of the samples were randomly selected for model training, while the remaining 30% were reserved for independent accuracy assessment (Figure 2). To assess the stability and variability of the classification results, the classification process was repeated 20 repetitions using different random seeds. To assess the stability and variability of the classification results, the classification process was repeated 20 times using different random seeds, while maintaining a minimum distance of 500 m between reference samples. The mean and standard deviation (*SD*) of the overall accuracy (*OA*), *Kappa coefficient,* producer's accuracy (*PA*), and user's accuracy (*UA*) were then calculated from the 20 independent runs.

3.2.2 Image classification

LULC maps serve as a vital foundation for evaluating the spatial and temporal dynamics of the Earth's surface. To ensure consistency across sensors (TM, OLI and OLI-2), six equivalent optical spectral bands, including Blue, Green, Red, Near-Infrared (NIR), SWIR-1, and SWIR-2, were extracted to generate a multispectral composite image. Although the thermal infrared bands were subjected to scale-factor normalization during the preprocessing step, all thermal bands were completely excluded from the classification feature space. In this study, LULC maps were generated from Landsat satellite imagery by integrating optical spectral bands, spectral indices, and ancillary data with RF, CART, GTB, and SVM algorithms implemented on the GEE platform. These ML approaches are widely applied in LULC classification due to their high accuracy [28][29][30] and [31]. While spectral bands reflect the reflectance characteristics of surface features, spectral indices and ancillary data provide supplementary information that enhances the identification and discrimination of different LULC classes in remote sensing imagery [32]. The calculated spectral indices integrated into the input dataset included the Normalized Difference Vegetation Index (*NDVI*), Modified Normalized Difference Water Index (*MNDWI*), Normalized Difference Built-up Index (*NDBI*), and Soil Adjusted Vegetation Index (*SAVI*). *NDVI* is defined in Equation (3), *MNDWI* in Equation (4), *NDBI* in Equation (5), and *SAVI* in Equation (6) [33][34][35] and [36], alongside slope and elevation values [10]. These indices were selected to characterize biological, topographic, hydrological, and vegetation density features, thereby improving the discriminative capability among LULC types during the classification process [37].

$$NDVI = \frac{NIR - RED}{NIR + RED}$$

Equation 3

$$MNDWI = \frac{Green - SWIR1}{Green + SWIR1}$$

Equation 4

$$NDBI = \frac{SWIR1 - NIR}{SWIR1 + NIR}$$

Equation 5

$$SAVI = \frac{NIR - RED}{NIR + RED + L}(1 + L)$$

Equation 6

Where *RED*, and *Green*, represent the wavelengths in the visible spectrum; *NIR* denotes the near-infrared wavelength; *SWIR1* refers to the shortwave infrared wavelength within the 1.55 - 1.75 μm range; and L = 0.5.

This research aims to improve LULC mapping precision by leveraging advanced ML classifiers hosted on the GEE platform. First, a suite of 600 reference points per year was integrated into the GEE environment. The collected samples were randomly divided into training (70%) and validation (30%) datasets for LULC mapping Four ML algorithms, namely RF, CART, GTB, and SVM, were tested to categorize LULC types in Phu Quoc. To identify the optimal results and ensure the accuracy and reliability of the LULC classification process when comparing different ML algorithms, each algorithm was tested using different classification parameter settings, and the parameter setting that achieved the highest reliability was selected (Table 5).

Table 5: Selected hyperparameter values for RF, CART, GTB, and SVM classifiers

Classifier	Hyperparameter	Search Space/Range	Selected Optimal Value
Random Forest	numberOfTrees	100 - 500	200
	minLeafPopulation	1 - 10	1
Support Vector Machine	kernelType	RBF, LINEAR, POLY	RBF
	cost (C)	0.1, 1, and 10	10
	gamma	0.1, 0.5, and 1.0	0.5
Gradient Tree Boost	numberOfTrees	100 - 300	100
	shrinkage	0.005, 0.01, and 0.1	0.01
	samplingRate	0.2, 0.3, and 1.0	1.0
Classification and Regression Trees	maxNodes	20, 50, 100, and unrestricted (null)	null
	minLeafPopulation	1 - 5	3

The classification models were trained using a comprehensive input matrix encompassing Landsat satellite spectral bands, calculated spectral indices *(NDVI, MNDWI, NDBI, and SAVI),* and auxiliary predictors. Following the training phase, LULC maps were produced for each algorithm. To assess classification performance, the outputs were validated against an independent testing sample set through a confusion matrix. The performance of the models was systematically evaluated using standard accuracy metrics, including overall accuracy *(OA)* and the *Kappa coefficient*.

3.2.3 Accuracy assessment

The classification results were evaluated using overall accuracy *(OA)* and the *Kappa coefficient (Kappa)*. *OA* was calculated as the ratio of correctly classified samples (*TP*) to the total number of validation samples (*N*) as presented in Equation 7, whereas the *Kappa coefficient* (κ) measures the agreement between the classification results and reference data while accounting for agreement occurring by chance (Equation 8). These metrics were employed to assess, and compare the performance of the RF, CART, GTB, and SVM algorithms within the GEE platform.

$$OA = \frac{TP}{N} \times 100$$

Equation 7

$$\kappa = \frac{p_o - p_e}{1 - p_e}$$

Equation 8

Where p_o is the observed agreement, and p_e is expected agreement

The accuracy of individual LULC classes was assessed using producer's accuracy *(PA)* and user's accuracy *(UA)*, calculated from the confusion matrix according to Equations (9) and (10) [38]. These metrics provide detailed insights into omission and commission errors for each LULC class:

$$PA = \frac{x_{ii}}{n_i} \times 100$$

Equation 9

Where x_{ii} is the number of correctly classified pixels in row *i* and column *i* (the diagonal value for class *i*). And n_i is the total number of reference (ground truth) pixels or samples for class *i* (the column total).

$$UA = \frac{x_i}{x_{i+}} \times 100$$

Equation 10

Where x_i is the true positives for class i. And x_{i+} is the total number of samples classified as class *i* (the row sum or total predicted/mapped as class *i*)

To assess the stability and variability of the classification results, rather than reporting only the metrics obtained from a single run *(OA, Kappa, PA and UA),* we implemented a repeated random sub-sampling validation procedure with 20 repetitions on the GEE platform. Validation points overlapping the 500 m buffer around the training points were removed, ensuring that the remaining validata points were located at least 500 m away from the training points. This procedure was used to determine the mean *(OA, K, PA and UA)* ± *standard deviation (SD)* of the accuracy metrics (Equation 11).

$$SD = \sqrt{\frac{\sum_{i=1}^{n} \left(x_i - \bar{x}\right)^2}{n-1}}$$

Equation 11

Where n = sample size, x = Each value from the sample, $\bar{x}$ = The sample mean.

The performance of the RF, CART, GTB, and SVM classification algorithms was compared descriptively based on the accuracy metrics obtained from the repeated validation procedure. The most accurate LULC map produced by the selected algorithm was further validated through visual interpretation using high-resolution Google Earth satellite imagery.

3.2.4 Change detection

The selected post-classification LULC maps were exported to Google Drive and processed in ArcGIS, where they were reprojected into the WGS 84/UTM Zone 48N coordinate system. The purpose of this transformation was to ensure the spatial consistency of the LULC maps for accurate change detection analysis. LULC changes throughout the 30-year study period (1995-2025) were quantified by comparing the classification maps of different years. Subsequently, a change matrix and a spatial change map were generated to determine the magnitude, direction, and spatial distribution of LULC transitions across the Phu Quoc.

4. Results

4.1 LULC Classification

The results of the four ML algorithms showed that forest was the predominant LULC type in the study area, with the following average percentages across the study years: RF (69.00%), CART (68.82%), GTB (70.34%), and SVM (68.23%). However, forest area exhibited a declining trend over the past 30 years, decreasing by 11.56%. Following forest, agricultural land was the second largest LULC type, reflecting the vital role of agricultural production activities on the island. Bare land ranked third, primarily comprising unutilized land, areas undergoing land leveling or excavation, and sandy beach. Meanwhile, built-up area was the fourth largest LULC category but showed a distinct increasing trend over time, closely linked to urbanization, infrastructure expansion, and tourism development. Water body accounted for the lowest proportion of the land-use structure, yet exhibited a slight upward trend throughout the study period (Figure 4).

Across the classification years, the area of agricultural land exhibited certain fluctuations among the algorithms due to differences in classification performance and spectral confusion with bare land or sparse vegetation classes. The misclassification rate of agricultural land was attributed to the fact that several cultivated areas were captured during the harvest season, thereby exhibiting spectral characteristics similar to those of bare land. Despite specific variations among the algorithms, the overall LULC changes trends were highly consistent, characterized by a decline in forest area, an increase in built-up area and water body, and negligible fluctuations in agricultural and bare lands. Forest was mainly concentrated in the northeastern and eastern parts of the island, whereas agricultural land and built-up area were largely distributed along the western coast (Figure 5).

The RF, CART, GTB, and SVM algorithms generally yielded satisfactory LULC classification results throughout the study years. However, visual inspection revealed that some discrepancies still existed among the algorithms. GTB tended to classify a larger forest area compared to the alternative algorithms, particularly in 2025, when some agricultural lands were misidentified as forest. Similarly, CART frequently confused agricultural land with bare land in 2005, while certain bare areas were classified as built-up area in 2025. For SVM, errors primarily occurred in some water body areas in 2005, where these features were misidentified as forest. These discrepancies indicate that the algorithms still face challenges in distinguishing LULC classes with similar spectral properties.

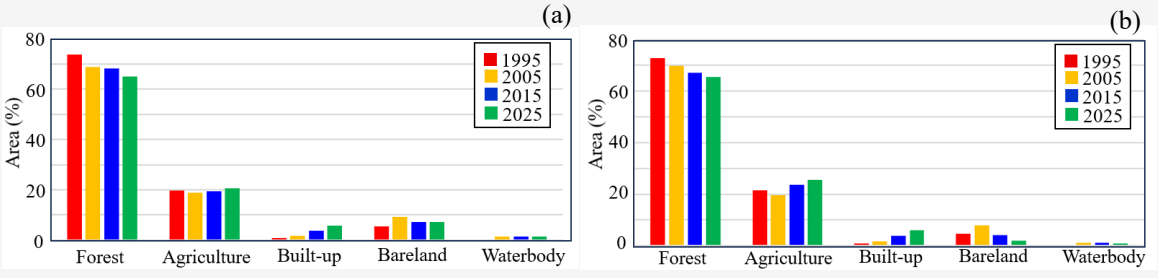


Figure 4: LULC areas in percentage in 1995, 2005, 2015 and 2025: (a) RF, (b) CART

(continue next page)

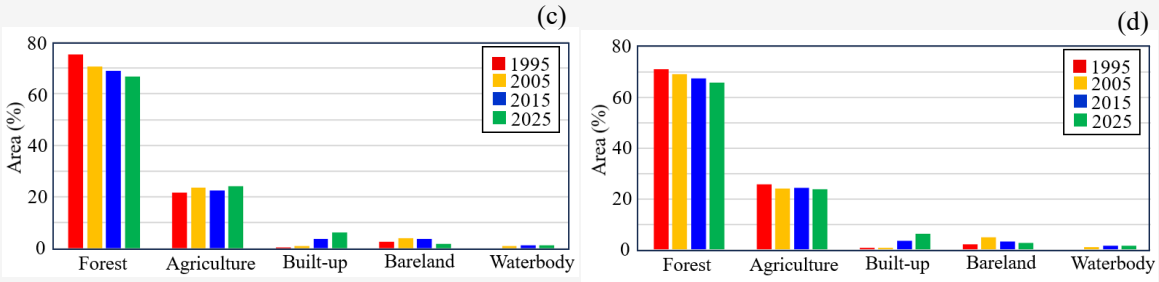


Figure 4: LULC areas in percentage in 1995, 2005, 2015 and 2025 (c) GTB, and (d) SVM
(Continue from previous page)

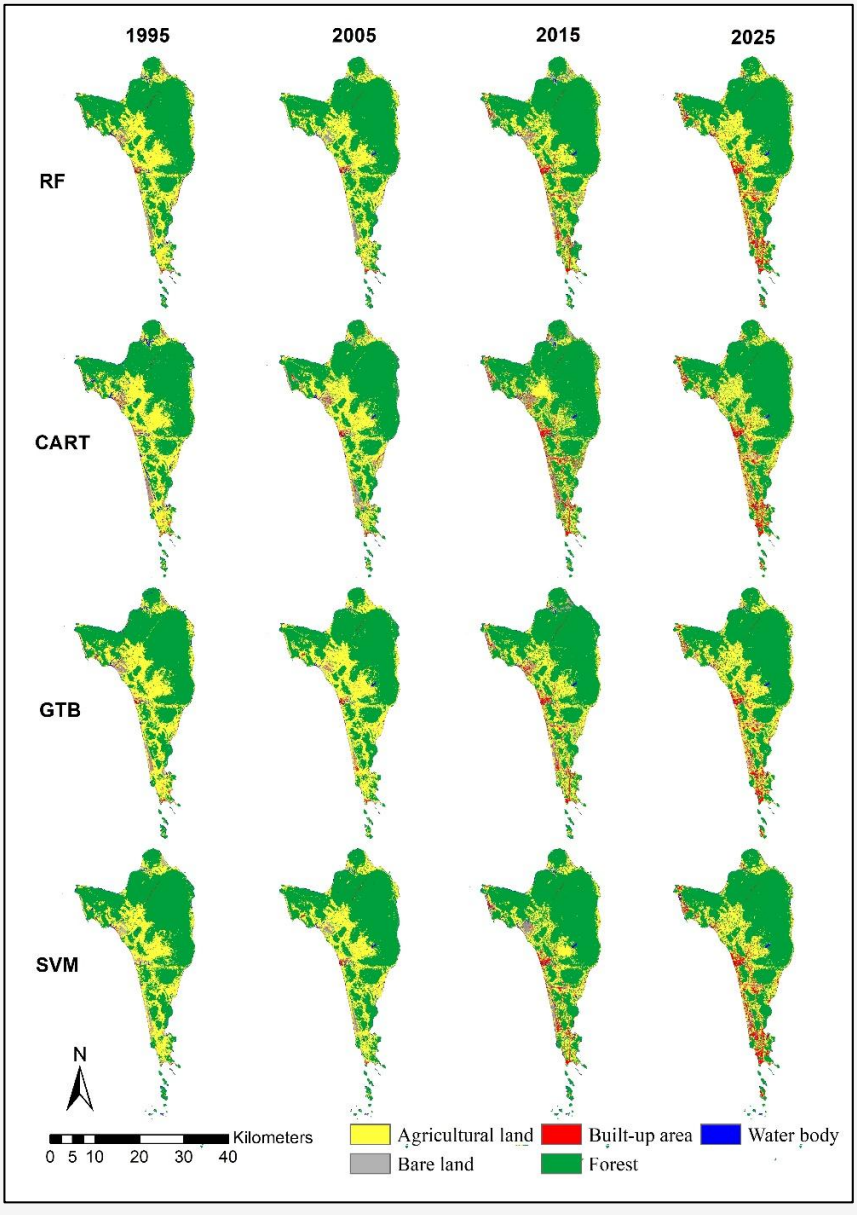


Figure 5: LULC classification maps of Phu Quoc produced by RF, CART, GTB, and SVM algorithms

4.2 Assessment of Classification Accuracy

4.2.1 Comparative performance of classification algorithms

In this study, the accuracy of the classification models was evaluated using a repeated resampling procedure with 20 repetitions, combined with a 500 m radius spatial distance filter between the training and validation datasets. The accuracy results for the four ML algorithms across the four study years are presented in Table 6. As shown in Table 6, all four ML algorithms achieved relatively high classification accuracy across the study years, although their performance varied among the algorithms and periods. The RF algorithm consistently showed the highest overall classification performance and the best stability throughout the four study years. The *OA* and *Kappa* values remained high, together with relatively small variations across repeated validation runs, indicating that RF was less affected by temporal differences in the Landsat data and produced more reliable classification results. SVM also showed good performance, particularly for the 2025 data, whereas CART and GTB showed greater variations in performance among the study years. These results indicate that RF was the most suitable algorithm among those evaluated for generating multi-temporal LULC maps for the study area. The class-level accuracy results also showed differences among the LULC classes. Water body and forest classes generally achieved higher *PA* and *UA* values across all algorithms and study years, indicating that these classes had more distinct spectral characteristics and were therefore easier to distinguish from other LULC classes in Landsat imagery. In contrast, agricultural land, built-up area, and bare land generally had lower *PA* and *UA* values and exhibited greater variation. The relatively high classification uncertainty for these classes may be attributed to their similar spectral characteristics, particularly when agricultural land, bare land, and sparsely built-up area were located close to one another. Such spectral and spatial heterogeneity may increase the likelihood of confusion among these classes, especially in the early periods when reference information was limited in both quantity and quality. The variation in class-level accuracy was also more pronounced for certain classes and periods. For example, the built-up area class showed higher uncertainty in the 1995 classification results, which may be related to the dispersed spatial distribution and relatively small size of residential areas during this period.

Table 6: Classification accuracy of the ML algorithms across the study years, based on PA, UA, OA, and Kappa

Classifier	LU LC	1995		2005		2015		2025	
		PA	**UA**	**PA**	**UA**	**PA**	**UA**	**PA**	**UA**
RF	FR	0.92±0.03	0.93±0.03	0.98±0.02	0.98±0.02	0.97±0.02	0.96±0.02	0.96±0.02	0.97±0.02
	AL	0.85±0.04	0.78±0.05	0.91±0.04	0.92±0.05	0.89±0.04	0.87±0.04	0.91±0.04	0.90±0.03
	BA	0.75±0.05	0.91±0.04	0.83±0.04	0.89±0.05	0.87±0.05	0.87±0.04	0.94±0.05	0.93±0.01
	BL	0.88±0.05	0.84±0.05	0.85±0.05	0.77±0.05	0.80±0.03	0.84±0.05	0.95±0.04	0.95±0.03
	WB	0.98±0.02	0.98±0.03	0.97±0.05	1.00±0.00	0.94±0.05	0.94±0.05	0.97±0.03	0.98±0.03
OA (%)			**88.45 ± 2.73**		**92.91 ± 1.55**		**91.06 ± 1.73**		**94.41 ± 1.59**
Kappa			**0.84 ± 0.03**		**0.90 ± 0.02**		**0.88 ± 0.02**		**0.93 ± 0.02**
CART	FR	0.91±0.04	0.88±0.04	0.97±0.02	0.96±0.03	0.94±0.03	0.93±0.03	0.95±0.03	0.93±0.03
	AL	0.75±0.07	0.79±0.04	0.89±0.06	0.89±0.05	0.83±0.05	0.77±0.05	0.84±0.05	0.86±0.06
	BA	0.74±0.07	0.82±0.08	0.81±0.07	0.81±0.09	0.81±0.04	0.84±0.07	0.90±0.06	0.92±0.05
	BL	0.85±0.07	0.86±0.07	0.77±0.09	0.76±0.08	0.70±0.08	0.77±0.07	0.92±0.05	0.91±0.08
	WB	0.98±0.03	0.98±0.02	0.93±0.06	0.98±0.03	0.90±0.08	0.94±0.05	0.94±0.04	0.95±0.05
OA (%)			**85.92 ± 4.05**		**89.91 ± 2.21**		**87.86 ± 2.63**		**91.17 ± 2.68**
Kappa			**0.81 ± 0.05**		**0.86 ± 0.03**		**0.81 ± 0.03**		**0.88 ± 0.04**
GTB	FR	0.88±0.05	0.90±0.05	0.90±0.03	0.92±0.04	0.98±0.01	0.96±0.01	0.93±0.03	0.93±0.04
	AL	0.79±0.08	0.76±0.07	0.85±0.04	0.83±0.07	0.87±0.04	0.87±0.04	0.80±0.05	0.76±0.04
	BA	0.82±0.09	0.86±0.06	0.88±0.07	0.92±0.07	0.84±0.05	0.85±0.05	0.89±0.05	0.87±0.06
	BL	0.91±0.07	0.92±0.07	0.87±0.08	0.81±0.09	0.75±0.06	0.79±0.06	0.79±0.06	0.84±0.08
	WB	0.96±0.05	0.96±0.05	0.96±0.04	0.99±0.03	0.95±0.05	0.97±0.04	0.94±0.05	0.96±0.04
OA (%)			**86.68 ± 2.91**		**88.53 ± 2.25**		**90.12 ± 2.25**		**87.05 ± 1.88**
Kappa			**0.82 ± 0.04**		**0.84 ± 0.03**		**0.87 ± 0.03**		**0.83 ± 0.03**
SVM	FR	0.87±0.03	0.89±0.04	0.94±0.02	0.96±0.02	0.97±0.02	0.89±0.03	0.96±0.02	0.95±0.02
	AL	0.73±0.05	0.71±0.08	0.95±0.04	0.85±0.04	0.79±0.05	0.84±0.05	0.86±0.03	0.89±0.05
	BA	0.86±0.07	0.94±0.05	0.88±0.04	0.91±0.05	0.87±0.05	0.89±0.04	0.97±0.02	0.91±0.03
	BL	0.94±0.07	0.97±0.04	0.86±0.05	0.79±0.07	0.74±0.08	0.80±0.07	0.87±0.08	0.91±0.06
	WB	0.98±0.03	0.85±0.06	0.86±0.06	1.00±0.00	0.94±0.06	0.96±0.04	0.86±0.03	0.97±0.04
OA (%)			**86.47 ± 2.75**		**90.65 ± 1.83**		**87.60 ± 1.42**		**92.67 ± 1.96**
Kappa			**0.82 ± 0.03**		**0.87 ± 0.03**		**0.83 ± 0.02**		**0.90 ± 0.02**

Note: Forest (FR), Agricultural land (AL) Built-up area (BA), Bare land (BL) and Water body (WB)

This characteristic increased the likelihood of mixed pixels in the medium-resolution Landsat imagery and may have reduced the ability to distinguish built-up area from surrounding agricultural land or bare land. However, the *PA* and *UA* values generally remained above 0.70 for all LULC classes, indicating an acceptable level of classification accuracy for multi-temporal mapping in this study.

Overall, the *Kappa* coefficients of the LULC classification results were all above 0.80 across all study years, meeting the thresholds proposed by Landis and Koch [39] for LULC mapping using remote sensing imagery. Among the evaluated algorithms, RF showed the most stable performance, further supporting previous studies that have demonstrated the effectiveness of RF for LULC classification using remote sensing data [40] and [41]. The superior stability of RF across the study years also provided a basis for selecting this algorithm to generate LULC maps for subsequent analyses of LULC changes in Phu Quoc during the 1995-2025 period.

4.2.2 Qualitative visual verification using Google Earth imagery

For qualitative visual verification of the LULC map against high-resolution Google Earth imagery, the 2025 LULC map generated using the RF algorithm was selected. This map was selected because the RF algorithm showed higher reliability than the other algorithms, with *OA* (88.45 ± 2.73% to 94.41 ± 1.59%) and *Kappa* (0.84 ± 0.03 to 0.93 ± 0.02). In addition, high-resolution Google Earth imagery was available for the recent period, providing suitable visual reference information for qualitative comparison. In contrast, historical high-resolution Google Earth imagery for the earlier target years (1995 and 2005) was unavailable or insufficient to support a comparable visual assessment. Figure 6 presents a qualitative visual comparison between the 2025 RF classification and the corresponding Google Earth imagery at representative locations. The comparison indicated that the classified land cover types generally corresponded well with the spatial patterns observed in the reference imagery. Agricultural land at location A exhibited a similar spatial distribution in the classification and reference imagery. Built-up area at location B were generally consistent with the distribution of buildings and infrastructure visible in the Google Earth imagery. At location C, the non-vegetated areas corresponding to bare land were also visually captured by the classification. The water body at location D, particularly the reservoir area, showed a clear spatial correspondence between the classified and reference images. Similarly, the forest class at location E displayed a generally consistent spatial pattern with the corresponding Google Earth imagery. Some localized discrepancies were observed, particularly along transition zones between adjacent land cover types. Overall, this qualitative visual verification provides additional visual evidence of the spatial plausibility of the 2025 RF classification and complements the quantitative accuracy assessment reported in Table 6.

4.3 LULC Changes

In this study, the ML algorithms RF, SVM, CART, and GTB were used to classify LULC in Phu Quoc. The accuracy assessment results indicated that RF achieved higher accuracy than the other classifiers while maintaining stability across the studied years. Consequently, the LULC maps generated by the RF algorithm were selected for LULC changes analysis during the 1995-2025 period. The analysis of LULC changes was performed using ArcGIS software, a method that enables the determination of both the magnitude of change and the direction of transitions between LULC classes throughout the study period. The results showed that forest was the only land cover class experiencing a net loss, whereas all other land-cover classes exhibited net gains, with built-up area showing the largest positive net change (Figure 7). Specifically, a total area of 441.17 km² remained unchanged from 1995 to 2025. The key change during this period was the conversion of forest to agricultural land (40.92 km²), forest to built-up area (12.47 km²), agricultural land to bare land (25.26 km²), agricultural land to built-up area (14.49 km²), and bare land to agricultural land (12.88 km²) (Table 7) (Figure 8).

These results clearly reflect the effects of urban development, socio-economic growth, and tourism-related infrastructure on spatial LULC changes in Phu Quoc. Over the past three decades, numerous investments in transportation, urban infrastructure, and tourism services have increased the demand for converting land to built-up uses, such as residential areas, housing, resorts, and commercial centers. This has resulted in the expansion of existing built-up area and the decline of natural ecosystems. The findings of this study align with prior research in Phu Quoc, which demonstrated that tourism development and urbanization are the primary drivers of LULC changes on the island [10] and [11]. These findings are important considerations for land-use planning, land management, and land development to help prevent ecosystem degradation caused by urbanization.

Table 7: LULC transition matrix (1995-2025, km²)

LULC	Forest	Agricultural land	Built-up area	Bare land	Water body	Total 1995
Forest	361.03	40.92	12.47	1.97	0.61	417.00
Agricultural land	6.89	63.19	14.49	25.26	2.50	112.33
Built-up area	0.10	0.24	3.65	0.51	0.01	4.51
Bare land	0.00	12.88	2.19	12.26	3.80	31.13
Water body	0.77	0.03	0.02	0.01	1.04	1.87
Total 2025	368.79	117.26	32.82	40.01	7.96	566.84

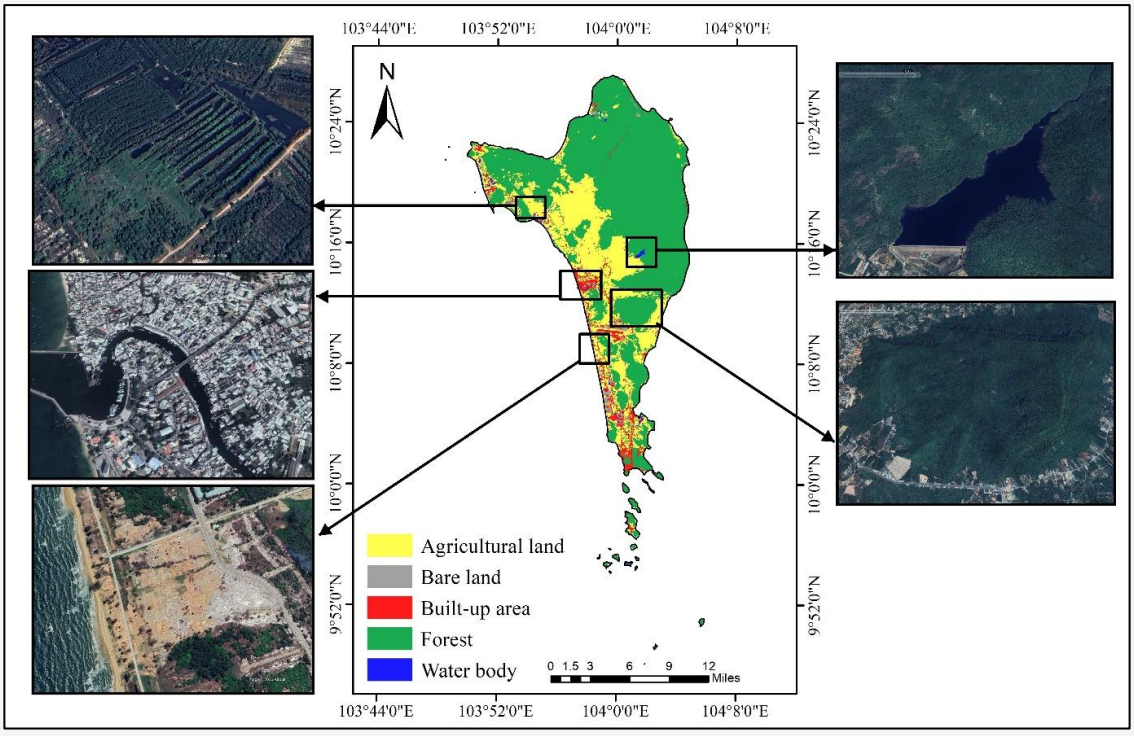


Figure 6: 2025 LULC validation using Google Earth

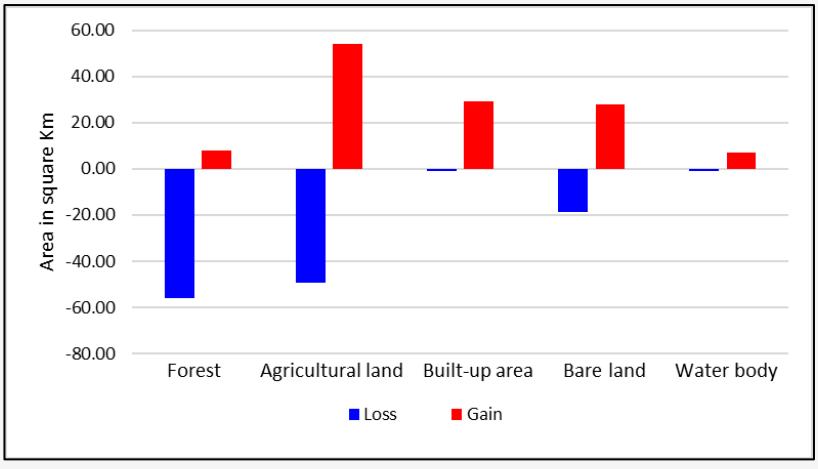


Figure 7: Gain and loss of LULC classes in Phu Quoc during 1995-2025

Consequently, the LULC maps generated by the RF algorithm were selected for LULC changes analysis during the 1995-2025 period. The analysis of LULC changes was performed using ArcGIS software, a method that enables the determination of both the magnitude of change and the direction of transitions between LULC classes throughout the study period. The results showed that forest was the only land cover class experiencing a net loss, whereas all other land-cover classes exhibited net gains, with built-up area showing the largest positive net change (Figure 7). Specifically, a total area of 441.17 km² remained unchanged from 1995 to 2025. The key change during this period was the conversion of forest to agricultural land (40.92 km²), forest to built-up area (12.47 km²), agricultural land to bare land (25.26 km²), agricultural land to built-up area (14.49 km²), and bare land to agricultural land (12.88 km²) (Table 7) (Figure 8).

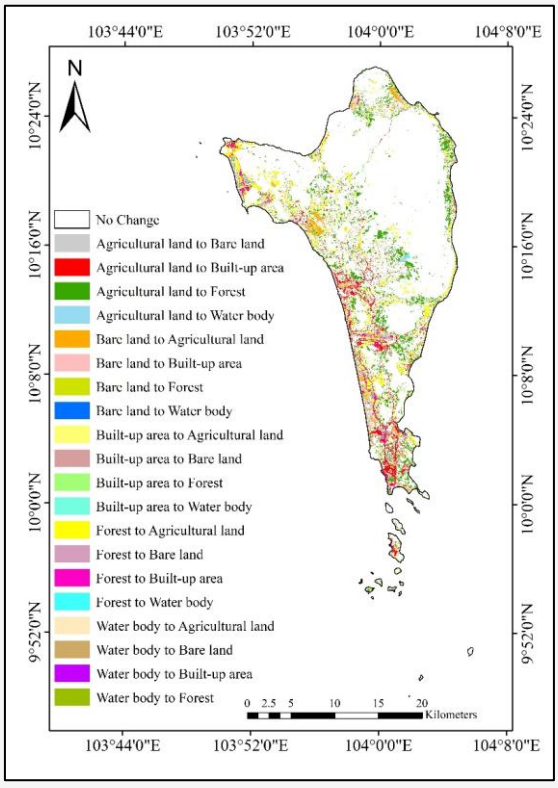


Figure 8: LULC transition from 1995 to 2025

These results clearly reflect the effects of urban development, socio-economic growth, and tourism-related infrastructure on spatial LULC changes in Phu Quoc. Over the past three decades, numerous investments in transportation, urban infrastructure, and tourism services have increased the demand for converting land to built-up uses, such as residential areas, housing, resorts, and commercial centers. This has resulted in the expansion of existing built-up area and the decline of natural ecosystems. The findings of this study align with prior research in Phu Quoc, which demonstrated that tourism development and urbanization are the primary drivers of LULC changes on the island [10] and [11]. These findings are important considerations for land-use planning, land management, and land development to help prevent ecosystem degradation caused by urbanization.

4.4 Limitations of the Study

Although the use of Landsat imagery on the GEE platform, together with ML algorithms such as RF, CART, GTB, and SVM, has demonstrated effective LULC classification performance, this approach still has certain limitations. Differences between sensors across Landsat satellite generations may lead to inconsistencies and affect the accuracy of LULC classification in Phu Quoc. Spectral indices have helped improve the distinction between characteristic LULC classes, such as those found in Phu Quoc National Park and residential areas; however, they may not adequately represent complex and heterogeneous LULC patterns. This limitation is particularly evident in agricultural land and areas where bare land is interspersed with vegetation. In addition, ML algorithms have varying sensitivities to the quality of training data, class imbalance (e.g., water body or bare land occupying relatively small proportions of the study area), and overfitting, which may result in inconsistent classification performance across different LULC classes.

Future studies should focus on higher-resolution and multi-source data, such as Sentinel-1, Sentinel-2, and other radar data, to improve the accuracy of LULC classification. More extensive analysis of multi-temporal imagery, together with the use of deep learning methods, could provide a better understanding of spatial distribution characteristics and temporal changes, thereby improving classification performance. In addition, the importance of input variables should be examined to determine their contributions to the discrimination of specific LULC classes, providing a basis for selecting a suitable classification model. Finally, increasing the number of field samples could improve the quality of the training data and increase the reliability of validation in future studies.

5. Conclusions

This study evaluated LULC changes in Phu Quoc during the period 1995-2025 by integrating Landsat imagery, Google Earth Engine, and four ML algorithms: RF, CART, GTB, and SVM. The comparison of the four classifiers showed that all methods were capable of producing reliable LULC

maps; however, RF provided the most stable and consistent performance across the study years. Therefore, the LULC maps generated using the RF algorithm were selected as the basis for subsequent analyses of change detection and spatial transitions. Multi-temporal analysis revealed clear changes in the LULC structure of Phu Quoc over the past three decades. Forest remained dominant but showed an overall decreasing trend, while built-up area experienced the strongest expansion. The main conversion processes included the conversion of forest and agricultural land to built-up area, along with reciprocal changes between agricultural land and bare land, while water body increased slightly during the study period.

The results demonstrate that integrating multi-temporal Landsat imagery with machine learning algorithms and GEE is an effective approach for monitoring LULC changes. This study contributes to the LULC analysis literature by providing a long-term and spatially detailed assessment of Phu Quoc, while systematically comparing machine learning algorithms to identify a suitable classification method for multi-temporal mapping. At the same time, the findings can support land-use planning, environmental management, forest conservation, and the development of sustainable development strategies for Phu Quoc. In addition, this methodological framework can be adapted for application in other areas experiencing rapid urbanization, particularly where long-term remote sensing data are available but historical land-use data are limited.

References

[1] Adepoju, M., Millington, A. and Tansey, K., (2006). Land Use/Land Cover change Detection in Metropolitan Lagos (Nigeria): 1984-2002. *ASPRS 2006 Annual Conference*, May 1-5, 2006, Reno, Nevada.

[2] Lambin, E. F., Turner, B. L., Geist, H. J., Agbola, S. B., Angelsen, A., Bruce, J. W., Coomes, O. T., Dirzo, R., Fischer, G., Folke, C., George, P. S., Homewood, K., Imbernon, J., Leemans, R., Li, X., Moran, E. F., Mortimore, M., Ramakrishnan, P. S., Richards, J. F., Skånes, H., Steffen, W., Stone, G. D., Svedin, U., Veldkamp, T. A., Vogel, C. and Xu, J., (2001). The Causes of Land-Use and Land-Cover Change: Moving Beyond the Myths. *Global Environmental Change*, Vol. 11(4); 261-269. https://doi.org/10.1016/S0959-3780(01)00007-3.

[3] Seyam, M. M. H., Haque, M. R. and Rahman, M. M., (2023). Identifying the Land Use Land Cover (LULC) changes Using Remote Sensing and GIS Approach: A Case Study at Bhaluka in Mymensingh, Bangladesh. *Case Studies in Chemical and Environmental Engineering*, Vol. 7. https://doi.org/10.1016/j.cscee.2022.100293.

[4] Wang, Z., Wang, T., Zhang, X., Wang, J., Yang, Y., Sun, Y., Guo, X., Wu, Q., Nepovimova, E., Watson, A. E. and Kuca, K., (2024). Biodiversity Conservation in the Context of Climate Change: Facing Challenges and Management Strategies. *Science of The Total Environment*, Vol. 937. https://doi.org/10.1016/j.scitotenv.2024.173377.

[5] Follmann, A., Kennedy, L., Pfeffer, K. and Wu, F., (2023). Peri-Urban Transformation in the Global South: A Comparative Socio-Spatial Analytics Approach. *Regional Studies*, Vol. 57(3); 447-461. https://doi.org/10.1080/00343404.2022.2095365.

[6] Moukomla, S. and Marome, W., (2025). Tourism-Induced Urbanization In Phuket Island, Thailand (1987–2024): A Spatiotemporal Analysis. *Urban Science*, Vol. 9(3). https://doi.org/10.3390/urbansci9030055.

[7] Lin, T., Xue, X., Shi, L. and Gao, L., (2013). Urban Spatial Expansion and Its Impacts on Island Ecosystem Services and Landscape Pattern: A Case Study of the Island City of Xiamen, Southeast China. *Ocean & Coastal Management*, Vol. 81; 90-96. https://doi.org/10.1016/j.ocecoaman.2012.06.014.

[8] Fu, T., Zhang, L., Chen, B. and Yan, M., (2022). Human Disturbance on the Land Surface Environment in Tropical Islands: A Remote Sensing Perspective. *Remote Sensing*, Vol. 14(9). https://doi.org/10.3390/rs14092100

[9] Quyet, L. V., Duy, P. T. and Toan, V. P., (2022). Sustainable Development of Tourism Economy in Phu Quoc Island, Kien Giang Province, Vietnam: Current Situation and Prospects. IOP Conference Series: *Earth and Environmental Science*, Vol. 1028(1). https://doi.org/10.1088/1755-1315/1028/1/012005.

[10] Nguyen, C. T., Downes, N. K., Sitthi, A. and Losiri, C., (2025). Tourism-Induced Land Use Transformations, Urbanisation, and Habitat Degradation in the Phu Quoc Special Economic Zone. *Urban Science*, Vol. 9(1). https://doi.org/10.3390/urbansci9010011.

[11] Thien, B. B., Kuznetsov, A. N. and Phuong, V. T., (2024). Monitoring Land Use/Land Cover Change Using Remote Sensing and GIS Techniques in Phu Quoc Island, Kien Giang Province, Vietnam. *Nexo Revista Científica*, Vol. 37(01); 83-98. https://doi.org/10.5377/nexo.v37i01.18331.

[12] National Assembly of Vietnam., (2017). *Law on Planning (Law No. 21/2017/QH14).* [Online]. Available: https://vanban.chinhphu.vn/?pageid=27160&docid=192206. [Accessed: Feb. 2, 2026].

[13] Moulds, S., Buytaert, W. and Mijic, A., (2018). A Spatio-Temporal Land Use and Land Cover Reconstruction for India from 1960-2010. *Scientific Data*, Vol. 5(1). https://doi.org/10.1038/sdata.2018.159.

[14] Kien Giang Provincial People's Committee., (2024). *Plan No. 86/KH-UBND on Land Registration and Initial Issuance of Land Use Rights Certificates in Phu Quoc City, Kien Giang Province.* [Online]. Available: https://thuvienphapluat.vn/van-ban/Bat-dong-san/Ke-hoach-86-KH-UBND-2024-cap-giay-chung-nhan-quyen-su-dung-dat-lan-dau-Phu-Quoc-Kien-Giang-605463.aspx. [Accessed: Feb. 2, 2026].

[15] Thammaboribal, P., and Tripathi, N. (2024). Predicting Land Use and Land Cover Changes in Pathumthani, Thailand: A Comprehensive Analysis from 2013 to 2023 Using Landsat Satellite Imagery and CA-ANN Algorithm, with Projections for 2028 and 2038. *International Journal of Geoinformatics*, Vol. 0(5), 13–27. https://doi.org/10.52939/ijg.v20i5.3225.

[16] Rogan, J. and Chen, D., (2004). Remote Sensing Technology for Mapping and Monitoring Land-Cover and Land-Use Change. *Progress in Planning*, Vol. 61(4); 301-325. https://doi.org/10.1016/S0305-9006(03)00066-7.

[17] Tran, T., Julian, J. and De Beurs, K., (2014). Land Cover Heterogeneity Effects on Sub-Pixel and Per-Pixel Classifications. *ISPRS International Journal of Geo-Information*, Vol. 3(2); 540-553. https://doi.org/10.3390/ijgi3020540.

[18] Maxwell, A. E., Warner, T. A. and Fang, F., (2018). Implementation of Machine-Learning Classification in Remote Sensing: An Applied Review. *International Journal of Remote Sensing*, Vol. 39(9); 2784-2817. https://doi.org/10.1080/01431161.2018.1433343.

[19] Tassi, A. and Vizzari, M., (2020). Object-Oriented LULC Classification in Google Earth Engine Combining SNIC, GLCM, and Machine Learning Algorithms. *Remote Sensing*, Vol. 12(22). https://doi.org/10.3390/rs12223776.

[20] National Assembly of Vietnam., (2025). *Resolution No. 1654/NQ-UBTVQH15 of the Standing Committee of the National Assembly: On the Rearrangement of Commune-Level Administrative Units in An Giang Province in 2025.* The Standing Committee of the National Assembly: Hanoi, Vietnam. [Online]. Available: https://vanban.chinhphu.vn/?pageid

[21] =27160&docid=214010. [Accessed: Feb. 2, 2026].

[22] U.S. Geological Survey., (2008). *Opening the Landsat Archive. USGS Fact Sheet 2008-3091*. https://doi.org/10.3133/fs20083091.

[23] U.S. Geological Survey. *Landsat Collection 2 Surface Reflectance*. [Online]. Available: https://www.usgs.gov/landsat-missions/landsat-collection-2-surface-reflectance. [Accessed: Dec. 19, 2025].

[24] Pimple, U., Sitthi, A., Simonetti, D., Pungkul, S., Leadprathom, K. and Chidthaisong, A., (2017). Topographic Correction of Landsat TM-5 and Landsat OLI-8 Imagery to Improve the Performance of Forest Classification in the Mountainous Terrain of Northeast Thailand. *Sustainability*, Vol. 9(2). https://doi.org/10.3390/su9020258.

[25] Phan, T. N., Kuch, V. and Lehnert, L. W., (2020). Land Cover Classification Using Google Earth Engine and Random Forest Classifier - The Role of Image Composition. *Remote Sensing*, Vol. 12(15). https://doi.org/10.3390/rs12152411.

[26] Ministry of Natural Resources and Environment., (2024). *Regulations on Land Statistics, Land Inventory, and Mapping of Current Land-Use Status (Circular No. 08/2024/TT-BTNMT).* [Online]. Available: https://congbao.chinhphu.vn/van-ban/thong-tu-so-08-2024-tt-btnmt-42595.htm. [Accessed: Feb. 2, 2026].

[27] Tran, H., Tran, T. and Kervyn, M., (2015). Dynamics of Land Cover/Land Use Changes in the Mekong Delta, 1973–2011: A Remote Sensing Analysis of the Tran Van Thoi District, Ca Mau Province, Vietnam. *Remote Sensing*, Vol. 7(3); 2899-2925. https://doi.org/10.3390/rs70302899.

[28] Fortier, J., Rogan, J., Woodcock, C. E. and Runfola, D. M., (2011). Utilizing Temporally Invariant Calibration Sites to Classify Multiple Dates and Types of Satellite Imagery. *Photogrammetric Engineering & Remote Sensing*, Vol. 77(2); 181-189.

[29] De Oliveira Ferreira Silva, C., (2020). Classificação Supervisionada De Área Irrigada Utilizando Índices Espectrais De Imagens Landsat-8 Com Google Earth Engine. *IRRIGA*, Vol. 25(1); 160-169. https://doi.org/10.15809/irriga.2020v25n1p160-169.

[30] Krivoguz, D., Chernyi, S. G., Zinchenko, E., Silkin, A. and Zinchenko, A., (2023). Using Landsat-5 for Accurate Historical LULC Classification: A Comparison of Machine Learning Models. *Data,* Vol. 8(9). https://doi.org/10.3390/data8090138.

[31] Simarmata, N., Wikantika, K., Tarigan, T. A., Aldyansyah, M., Tohir, R. K., Fauzi, A. I. and Fauzia, A. R., (2025). Comparison of Random Forest, Gradient Tree Boosting, and Classification and Regression Trees for Mangrove Cover Change Monitoring Using Landsat Imagery. *The Egyptian Journal of Remote Sensing and Space Sciences*, Vol. 28(1); 138-150. https://doi.org/10.1016/j.ejrs.2025.02.002.

[32] Xiaoxue Wang, Xiangwei Gao, Yuanzhi Zhang, Xianyun Fei, Zhou Chen, Jian Wang, Yayi Zhang, Xia Lu and Huimin Zhao., (2019). Land-Cover Classification of Coastal Wetlands Using the RF Algorithm for Worldview-2 and Landsat 8 Images. *Remote Sensing*, Vol. 11(16). https://doi.org/10.3390/rs11161927.

[33] Faridatul, M. I. and Wu, B., (2018). Automatic Classification of Major Urban Land Covers Based on Novel Spectral Indices. *ISPRS International Journal of Geo-Information*, Vol. 7(12). https://doi.org/10.3390/ijgi7120453.

[34] Tucker, C. J., (1979). Red and Photographic Infrared Linear Combinations for Monitoring Vegetation. *Remote Sensing of Environment*, Vol. 8(2); 127-150. https://doi.org/10.1016/0034-4257(79)90013-0.

[35] Long, N., Oanh, N., and Dinh, N. (2025). Application of GIS and Google Earth Engine to Assess Built-up Area Changes during Urbanization in Hai Duong City, Hai Duong Province, Vietnam. *International Journal of Geoinformatics*, Vol. 21(11), 46–58. https://doi.org/10.52939/ijg.v21i11.4599.

[36] Zha, Y., Gao, J. and Ni, S., (2003). Use of Normalized Difference Built-Up Index in Automatically Mapping Urban Areas from TM Imagery. *International Journal of Remote Sensing*, Vol. 24(3); 583-594. https://doi.org/10.1080/01431160304987.

[37] Andita, A., and Hidayati, N. (2025). Assessing CO2 Absorption of Urban Trees Using NDVI, SAVI, and MSARVI in Salatiga, Indonesia. *International Journal of Geoinformatics*, Vol. 21(4), 18–34. https://doi.org/10.52939/ijg.v21i4.4063.

[38] Liu, Y., Yang, K., Peng, Z., Zou, T., Su, D., Sun, R. and Ma, J., (2025). Land Use and Land Cover Classification and Terrestrial Ecosystem Carbon Storage Changes in Vietnam Based on Sentinel Images. *Scientific Reports*, Vol. 15(1). https://doi.org/10.1038/s41598-025-04765-z.

[39] Nasiri, V., Deljouei, A., Moradi, F., Sadeghi, S. M. M. and Borz, S. A., (2022). Land Use and Land Cover Mapping Using Sentinel-2, Landsat-8 Satellite Images, and Google Earth Engine: A Comparison of Two Composition Methods. *Remote Sensing*, Vol. 14(9). https://doi.org/10.3390/rs14091977.

[40] Landis, J. R. and Koch, G. G., (1977). The Measurement of Observer Agreement for Categorical Data. *Biometrics,* Vol. 33; 159-174. https://doi.org/10.2307/2529310.

[41] Gündüz, H. İ., (2025). Land-Use Land-Cover Dynamics and Future Projections Using GEE, ML, and QGIS - MOLUSCE: A Case Study in Manisa. *Sustainability*, Vol. 17(4). https://doi.org/10.3390/su17041363.

[42] Al Farikhi, F. and Pramono, R. W. D., (2023). Perbandingan Algoritma Classification and Regression Tree (CART) Dan Random Forest (RF) Untuk Klasifikasi Penggunaan Lahan Klasifikasi Penggunaan Lahan Pada Google Earth Engine. *Jurnal Spatial Wahana Komunikasi Dan Informasi Geografi*, Vol. 23(2); 170-179. https://doi.org/10.21009/spatial.232.09.